MM Science Journal | www.mmscience.eu
ISSN 1803-1269 (Print) | ISSN 1805-0476 (On-line)
Special Issue | HSM 2025
18th International Conference on High Speed Machining
October 15-16, 2025, Metz, France
DOI: 10.17973/MMSJ.2025_12_2025157

HSM2025-44832

ADAPTIVE TOOL ECCENTRICITY COMPENSATION USING MACHINE TOOL FEED DRIVES

Kaan Bahtiyar[1], Levent Bozcu[1], Seyed Mahmood Shantiaeezade[1], Burak Sencer*[1]
Ryosuke Ikeda[2] and Norikazu Suzuki[3]
[1]Oregon State University, Corvallis, USA.
[2]Mitsubishi Electric, Amagasaki, Japan
[3]Kobe University, Kobe, Japan
*Corresponding author; e-mail: burak.sencer@oregonstate.edu

Abstract
Eliminating tool eccentricity is critical for longer tool-life and high-quality surface finish. This paper presents an on-machine eccentricity cancellation strategy using machine tool feed drives. Circular motion at the spindle frequency is commanded to the feed axes to introduce an artificial eccentricity vector in tool coordinates. Cutting forces are monitored to extract the components induced by eccentricity in frequency domain, and an extremum seeking controller (ESC) is designed to cancel the eccentricity component by automatically adjusting the magnitude and orientation of the circular motion. Effectiveness of the proposed strategy is demonstrated in numerical simulations and machining experiments.
Keywords:
Tool eccentricity, adaptive compensation, feed drives

1 INTRODUCTION

Tool eccentricity is a well-known practical issue in milling operations. It deteriorates the surface roughness particularly in finishing operations and accelerates the tool wear in most milling applications leading to premature tool failure [Buj-Corral 2011, Schmitz 2004, 2007]. Eccentricity is primarily introduced during setting up the tool, and when the rotational axis of the tool and its geometric center become eccentric, circular trajectory of each tooth is altered, which leads to variations in the chip load and the cutting force. Another major cause for tool eccentricity is the runout of individual cutting inserts. Runout of an insert simply alters its circular trajectory as well, and on a tool with multiple inserts, the compound (vector sum of) teeth runout generates a resultant eccentricity effect [Sastry 2000].

Process models have been developed to predict the effect of eccentricity/runout on resultant cutting forces, surface finish as well as overall process stability [Buj-Corral 2011, Farhadmanesh 2021, Schmitz 2007, Takahei 2022]. To address the adverse effects, various strategies have also been developed. The most practical strategy is to eliminate runout during the tool assembly/mounting stage. Simple dial-gage based measurements can be taken, and the tool assembly can be adjusted by trial-and-error to eliminate runout. Nevertheless, due to thermal deformation, cutter dynamic imbalance, or simply because of uneven cutting edges, wear runout can initiate and lead to eccentricity. A more robust approach to eliminate runout is to implement on-machine and real-time compensation strategies.

One on-machine eccentricity suppression strategy is by making use of the sinusoidal spindle speed variation (SSV) functionality of modern machine tools [Sastry 2000]. SSV can vary the duration of a tooth in the cut, and this effect can be used to control the chip load. For instance, increasing the spindle speed around a tooth with a runout would help it regain its intended clip-load, and thus balance the overall cutting forces within a spindle revolution. This strategy has been demonstrated to suppress eccentricity induced force fluctuations up to 1500 rpm. Nevertheless, a key bottleneck of this strategy is that it requires the run-out/eccentricity parameters to be determined in-advance. The resultant eccentricity controls the SSV amplitude, and the alignment of the eccentricity vector with the cutting edge determines how the SSV command should be synchronized with the spindle rotation. Determining those parameters in-situ during the machining operation is challenging. Furthermore, such a strategy requires large modulation amplitude, which may not be applied due to the power limitations of the spindle servo system. Another strategy is to introduce feed modulations using the machine table so that the feedrate is lowered at the exact instance when a tooth with a runout is in-cut so that it removes chip at the desired feed-per-tooth level [Liang 1994, Stevens 1995]. This strategy requires the machine tool axes to undergo sinusoidal motion at spindle frequency, which can be accurately realized only up to 30-50 Hz, primarily limited by servo positioning bandwidths. Above that range, sinusoidal commands are greatly gain and phase modulated by the feed drive dynamics and if not compensated carefully, they may even worsen the tool eccentricity effect.

This paper proposes an adaptive feed modulation strategy using machine tool feed drives where i) tool eccentricity component is identified in-situ using the frequency spectrum of the cutting force or the machining vibration signals and ii) cancelled by sinusoidal feed modulations delivered by the machine tool feed drives whose parameters are adapted in real-time.

MM Science Journal | www.mmscience.eu
ISSN 1803-1269 (Print) | ISSN 1805-0476 (On-line)
Special Issue | HSM 2025
18th International Conference on High Speed Machining
October 15-16, 2025, Metz, France
DOI: 10.17973/MMSJ.2025_12_2025157

2 TOOL ECCENTRICITY COMPENSATION

2.1 Chip thickness with tool eccentricity

Firstly, let us consider a general helical tool with a helix angle (β) and N_f cutting flutes rotating at the angular spindle frequency of ω_{sp}. The rotation angle $\phi_{j,l}$ of the j^{th} cutting flute at the l=1…N_l^{th} layer along the tool height (H) can be expressed in time (t) as:

$$\phi_{j,l}(t) = \phi_0 + \omega_{sp} t - \frac{2\pi(j-1)}{N_f} - \frac{2a_p \tan(\beta)}{DN_l} H \qquad (1)$$

where $\phi_0 = 0$ is set for the reference tooth at $t = 0$. D is the tool diameter, and a_p is the axial depth of cut. The kinematics of milling tool with eccentricity (equivalent runout) is presented in Fig. 1a. As shown, tool's geometric center is shifted from its rotational center, by an eccentricity vector in the tool coordinates,

$$\boldsymbol{\delta}^t = \epsilon \begin{bmatrix} \cos\theta_\epsilon \\ \sin\theta_\epsilon \end{bmatrix}, \qquad (2)$$

which alters the cutting-edge trajectory causing fluctuation in the chip thickness. Radius of each (j^{th}) cutting edge can be computed by its nominal edge radius $r_{n,j}$ and the eccentricity vector [Takahei 2022] as:

$$r_j = |r_j| = |r_{n,j} + \boldsymbol{\delta}^t| = r_n + \epsilon\cos(\theta_e + \phi_{j,l}) \qquad (3)$$

and the instantaneous chip thickness can be evaluated by:

$$h_{j,l} = \left[\underbrace{h_n(\theta_{j,l})}_{nominal} + \underbrace{r_j - r_{j-1}}_{eccentricity} \right] g(\theta_{j,l}) \qquad (4)$$

where $h_n = csin(\theta_{j,l})$ is the nominal (commanded) chip thickness based on the feedrate c, whereas $r_i - r_{i-1}$ is the eccentricity component, which assumes that the material left from the previous $(j-1)^{th}$ tooth due to its eccentric trajectory is removed by the current (j^{th}) tooth. The function $g(\theta_{j,l})$ is defined as a windowing function to ensure that chip is removed when there is tooth engagement defined within the entry (θ_{st}) and exit angles (θ_{ex}):

$$g(\theta_{j,l}) = \begin{cases} 1, \theta_{st} \le \theta_{j,l} \le \theta_{ex} \\ 0, otherwise \end{cases} \qquad (5)$$

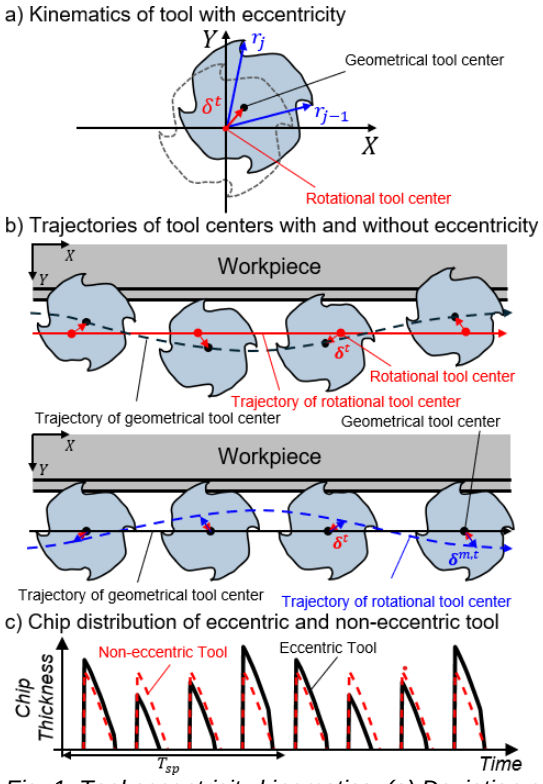

Fig. 1: Tool eccentricity kinematics. (a) Deviation of tool's rotational center. (b) Eccentricity schematic. (c) Eccentricity effect on the chip thickness.

Fig.1c shows the chip thickness variation. As shown, eccentricity induces a chip-load variation that is synchronized with the spindle period.

It can be also noted that the eccentricity vector can be projected onto the workpiece coordinates:

$$\boldsymbol{\delta}^{wp} = \begin{bmatrix} cos\,\omega_{sp}t & sin\,\omega_{sp}t \\ -sin\,\omega_{sp}t & cos\,\omega_{sp}t \end{bmatrix} \boldsymbol{\delta}^t \rightarrow \boldsymbol{\delta}^{wp} = \epsilon \begin{bmatrix} cos\,\omega_{sp}t + \theta_\epsilon \\ sin\,\omega_{sp}t + \theta_\epsilon \end{bmatrix} \qquad (6)$$

which simply describes that the tool's geometric center exhibits a circular motion at the spindle rotational frequency ω_{sp}. Machine tool feed drives can be used to generate a circular trajectory with the radius $a_m = \epsilon$ but with a phase of $\theta_m = \theta_\epsilon + \pi$ as:

$$\boldsymbol{\delta}^m = a_m \begin{bmatrix} cos(\omega_{sp}t + \theta_m) \\ sin(\omega_{sp}t + \theta_m) \end{bmatrix} \qquad (7)$$

to cancel that circular motion, i.e., to eliminate eccentricity induces chip-thickness variation. The key is to determine the radius $\boldsymbol{a_m}$ and the phase $\boldsymbol{\theta_m}$ of the circular motion adaptively so that machine tool feed drive dynamics are compensated, and tool eccentricity could be cancelled.

2.2 Adaptive compensation scheme

One approach is to develop a control strategy that automatically adjusts the circular motion parameters to minimize the eccentricity/runout component. In this work, an extremum seeking controller (ESC) strategy [Ariyur 2003], illustrated in Fig. 2a, is proposed to achieve this. ESC is a real-time, model-free optimization strategy that identifies optimal set of variables that minimizes a cost function. In this application, the optimization variables are the circular trajectory parameters; namely, the radius and the phase, and the cost (objective) function is designed to penalize tool eccentricity.

It is well-known that tool eccentricity introduces a frequency component at the spindle rotation frequency [Farhadmanesh 2021, Sastry 2000]. Hence, the cost function to minimize eccentricity can be postulated as the cutting force spectral energy evaluated at the spindle rotation frequency as:

$$J = \left| \frac{2}{L} \sum_{n=0}^{L-1} F(nT_s) e^{-j\omega_{sp} n T_s} \right| \qquad (8)$$

where the DFT of cutting force is evaluated based on the data collected within a single spindle revolution $L = 60/(T_s\omega_{sp})$ at the sampling rate of T_s.

To minimize the cost function (J), the ESC employs a gradient descent strategy where the optimization variables $\boldsymbol{\alpha} = [a_m, \theta_m]^T$ are updated along the gradient of the cost

MM Science Journal | www.mmscience.eu
ISSN 1803-1269 (Print) | ISSN 1805-0476 (On-line)
Special Issue | HSM 2025
18th International Conference on High Speed Machining
October 15-16, 2025, Metz, France
DOI: 10.17973/MMSJ.2025_12_2025157

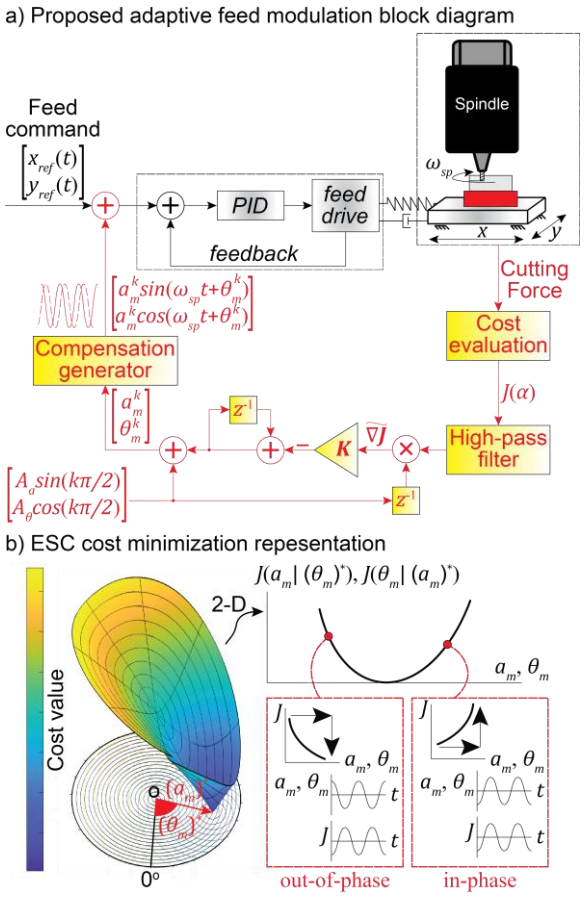

Fig. 2: ESC-based eccentricity cancellation. (a) Block diagram. (b) Cost function minimization strategy.

function with respect to optimization variables $\nabla \boldsymbol{J} = \frac{\delta J}{\delta \boldsymbol{\alpha}}$ by a fixed step size ($\boldsymbol{K}$) as:

$$\begin{bmatrix} \dot{a}_m \\ \dot{\theta}_m \end{bmatrix} = -\underbrace{\begin{bmatrix} K_a & 0 \\ 0 & K_\theta \end{bmatrix}}_{\boldsymbol{K}} \underbrace{\begin{bmatrix} \frac{\partial J}{\partial a_m} \\ \frac{\partial J}{\partial \theta_m} \end{bmatrix}}_{\widetilde{\nabla \boldsymbol{J}}} \tag{9}$$

The cost function gradient $\nabla \boldsymbol{J}$ is estimated in a data-driven manner by perturbing the process through modulation of the optimization variables and observing the cost function variation. Optimization variables are perturbed sinusoidally around their nominal value $\boldsymbol{\alpha_n}$ as:

$$\boldsymbol{\alpha} = \boldsymbol{\alpha_n} + \underbrace{\begin{bmatrix} A_a sin(\omega_p t + \Psi_a) \\ A_\theta sin(\omega_p t + \Psi_\theta) \end{bmatrix}}_{\boldsymbol{P}} \tag{10}$$

where $\boldsymbol{P}$ is the perturbation vector, ω_p is the perturbation frequency, A_a and A_θ are the perturbation amplitudes, and Ψ_a and Ψ_θ are the perturbation phases applied on the nominal optimization variables $\boldsymbol{\alpha_n}$, respectively. The cost function variation around $\boldsymbol{\alpha_n}$ can then be approximated using its Taylor series expansion:

$$J(\boldsymbol{\alpha}) = J(\boldsymbol{\alpha_n} + \boldsymbol{P}) \approx J(\boldsymbol{\alpha_n}) + \underbrace{\frac{\delta J(\boldsymbol{\alpha_n})}{\delta \boldsymbol{\alpha}}}_{\nabla \boldsymbol{J}^T} \boldsymbol{P} + H.O.T. \tag{11}$$

Notice in Eq.11 that the 1st term $J(\boldsymbol{\alpha_n})$ is its DC (nominal) component, while the 2nd term encodes how the gradient modulates the cost function due to the sinusoidal perturbations. By high-pass filtering the cost in Eq.11 and neglecting higher order terms ($H.O.T.$), it can be approximated as:

$$J_{HPF}(\boldsymbol{\alpha}) \approx \nabla \boldsymbol{J}^T \boldsymbol{P} \tag{12}$$

and its demodulation by the same sinusoidal perturbations $\boldsymbol{P}$ yields:

$$J_{HPF}(\boldsymbol{\alpha})\boldsymbol{P} \approx \nabla \boldsymbol{J}^T \boldsymbol{P}\boldsymbol{P} = \boldsymbol{P}\boldsymbol{P}^T \nabla \boldsymbol{J} = \begin{bmatrix} D_1 & D_{2,3} \\ D_{2,3} & D_4 \end{bmatrix} \begin{bmatrix} \frac{\partial J}{\partial a_m} \\ \frac{\partial J}{\partial \theta_m} \end{bmatrix} \tag{13}$$

where

$$\left.\begin{aligned} D_1 &= A_a^2 \sin^2(\omega_p t + \Psi_a) = \frac{A_a^2}{2}\left(1 - \cos\left(2(\omega_p t + \Psi_a)\right)\right) \\ D_{2,3} &= \frac{A_a A_\theta}{2}\left(\cos(\Psi_a - \Psi_\theta) - \cos(2\omega_p t + \Psi_a + \Psi_a)\right) \\ D_4 &= A_\theta^2 \sin^2(\omega_p t + \Psi_\theta) = \frac{A_\theta^2}{2}\left(1 - \cos\left(2(\omega_p t + \Psi_\theta)\right)\right) \end{aligned}\right\} \tag{14}$$

In Eq. 13, D_1 and D_4 scale each partial derivative by the perturbation amplitude squares, while $D_{2,3}$ capture cross-terms. The high-frequency components at $2\omega_p t$ vanish upon averaging over the dither period or with low-pass filtering Eq.13. If $\Psi_a - \Psi_a$ is selected to be integer multiplier of $\pi/2$, $D_{2,3}$ vanishes, and Eq.13 can be approximated to:

$$J_{HPF}(\boldsymbol{\alpha})\boldsymbol{P} \approx \begin{bmatrix} \frac{A_a^2}{2}\frac{\partial J}{\partial a_m} \\ \frac{A_\theta^2}{2}\frac{\partial J}{\partial \theta_m} \end{bmatrix} \tag{15}$$

It shows that he demodulated term $J_{HPF}(\boldsymbol{\alpha})\boldsymbol{P}$ provides a data-based estimate $\widetilde{\nabla \boldsymbol{J}}$ of the true gradient $\nabla \boldsymbol{J}$. In this application, since the cost is calculated using windowed data from the most recent spindle revolution, the optimization update is performed once per revolution. To facilitate this, the perturbation signal is implemented as discrete sine wave samples at the k^{th} optimization step, and the update rule for the optimization variables $\boldsymbol{\alpha}$ at each spindle period is given by:

$$\underbrace{\begin{bmatrix} a_m \\ \theta_m \end{bmatrix}^k}_{\boldsymbol{\alpha}} = \boldsymbol{\alpha}^{k-1} - \boldsymbol{K}\widetilde{\nabla \boldsymbol{J}} + \begin{bmatrix} A_a sin(k\pi/2) \\ A_\theta cos(k\pi/2) \end{bmatrix} \tag{16}$$

Fig. 2a depicts the overall block diagram of the control scheme. As shown, the DC component of the perturbed cost function (Eq.11) is removed by a high-pass filter, and the signal is then demodulated to provide the gradient estimate to the gradient descent update rule. The optimization variables are integrated with integrator gains (step sizes) K_a and K_θ. This integration also helps to attenuate the high-frequency terms in Eq.13 and increments optimization variables according to Eq.16.

Fig. 2b schematically illustrates the above-described process, showing how the estimated gradient guides the optimization variables toward their optimal values. The variation in the cost function becomes either in-phase or out-of-phase with respect to the sinusoidal perturbations, depending on whether the optimization variables are positioned above or below their optimal values. Multiplying the sinusoidally perturbed optimization variables by the

MM Science Journal | www.mmscience.eu
ISSN 1803-1269 (Print) | ISSN 1805-0476 (On-line)
Special Issue | HSM 2025
18th International Conference on High Speed Machining
October 15-16, 2025, Metz, France
DOI: 10.17973/MMSJ.2025_12_2025157

resulting cost variations generates a predominantly positive or negative signal, which indicates whether an increase in the optimization variables will lead to an increase or decrease in the cost value, respectively.

3 NUMERICAL VALIDATION

The proposed strategy is first tested using time-domain simulations using the model presented in Section 2. Two simulation cases are created with a 4-flute cutter with the diameter of 10 mm, 20% radial immersion, and feedrate of 80 µm/tooth (i.e., 374 and 576 mm/min, respectively). The rest of the simulation parameters are provided in Tab. ***1***.

Tab. 1: Numerical simulation parameters

Parameter	Case1	Case2	Unit
Spindle speed	1200	1800	[rpm]
Axial depth of cut	1	2	[mm]
Eccentricity amplitude	20	15	[µm]
Eccentricity phase	40	20	[deg]
Amplitude step size (K_A)	45	45	–
Perturbation Amplitude (A_a)	2	2	[µm]
Phase step size (K_θ)	50	50	–
Perturbation Amplitude (A_θ)	2	2	[deg]

Fig. 3 shows the time domain simulation under two different conditions (See Case1 and Case2 in Tab. ***1***). The initial tool eccentricity is detected by evaluating the cost function using the power spectrum at the first spindle frequency harmonic. Once the proposed adaptive algorithm is started (see "Adaptation start" in Fig3), it automatically adjusts the adaptation parameters towards their optimal values in both conditions. In Case 2, a higher spindle speed and depth of cut pair is used, while maintaining the same demodulation amplitudes and step sizes as in Case 1 to demonstrate the robustness of the parameter selection and validate the effectiveness of the algorithm. As shown, in both cases, the algorithm converges to the optimal values in ~10seconds

The convergence rate of the algorithm can be adjusted by selecting appropriate tuning of perturbation amplitudes and step sizes. Using a higher perturbation amplitude can accelerate convergence, but it comes at the cost of larger perturbations in the steady-state signals after convergence, while the adaptation (perturbation, i.e., dither signal) can be stopped at the mean value after convergence. Increasing the step sizes also accelerates convergence, but it could lead to instability if chosen excessively.

When the algorithm converges to the optimal values, the chip load and cutting force are equally distributed among the cutter's flutes. As a result, the force profile becomes periodic at the tooth-passing frequency which minimizes the first harmonic of the spindle frequency, i.e., the cost.

4 EXPERIMENTAL VALIDATION

Experiments are conducted on a 3-axis machine tool using a workpiece shown in Fig. 4a. The feed servo drives are controlled by PID position control, and feed modulation commands are added into the position loop (see Fig. 2a) at

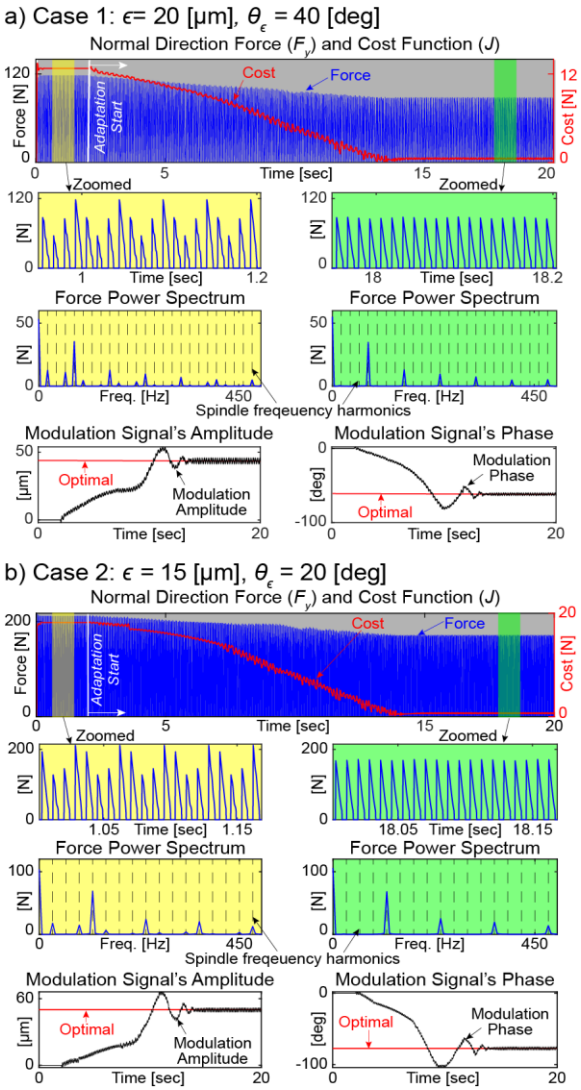

Fig. 3 : Numerical validations. (a) Case 1. (b) Case 2.

a sampling rate of 5 kHz. A 4-flute cutter with 10 mm diameter and 15% radial immersion, and feedrate of 75 µm/tooth (300 mm/min) is used to machine Al6061 alloy. The rest of the process parameters are given in Tab. ***2***.

Tab. 2: Experimental parameters

Parameter	Value	Unit
Spindle speed	1000	[rpm]
Axial depth of cut	2.5	[mm]
Amplitude step size (K_a)	40	–
Perturbation Amplitude (A_a)	1	[µm]
Phase step size (K_θ)	20	–
Perturbation Amplitude (A_θ)	2.5	[deg]

Fig. 4b shows the experimental results. The force data used for cost calculation is recorded using a dynamometer during the process. The cutting force in normal direction is used for the cost calculation, which is evaluated once per spindle revolution. The results show that as the algorithm reduces

MM Science Journal | www.mmscience.eu
ISSN 1803-1269 (Print) | ISSN 1805-0476 (On-line)
Special Issue | HSM 2025
18th International Conference on High Speed Machining
October 15-16, 2025, Metz, France
DOI: 10.17973/MMSJ.2025_12_2025157

the cost, the maximum force level is also decreased. It should be noted that after the algorithm converges, the cutting forces are distributed evenly among the cutter's flutes, which improves the final surface finish and extends the tool's lifetime.

An overshoot in modulation phase and amplitude is observed if the step size (adaptation gain) is selected too large. While smaller steps reduce overshoot, they slow convergence; larger steps on the other hand, accelerate convergence but causes oscillations and higher final costs due to persistent excitation of system. Besides, as the algorithm nears the optimum, reduced cost sensitivity may lead to suboptimal results. Adaptive step size adjustment can address this.

Another limitation is the effect of friction or mismatched feed drive dynamics in the feed and normal directions, which can distort circular motion and impair eccentricity compensation. Although the axis dynamics are matched at the spindle rotation frequency in this study, additional optimization variables can be introduced to compensate for gain and phase mismatches between feed and normal axis responses at the frequency of interest. This helps restore the intended circular motion and compensates for mismatch of axes dynamics and friction.

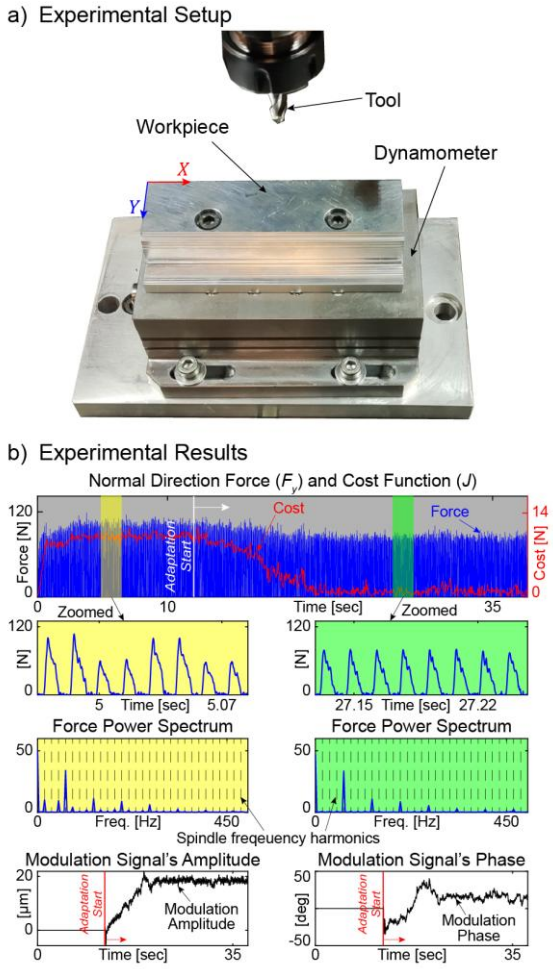

Fig. 4 : Experimental validation. (a) Setup. (b) Cutting force profiles and convergence trends.

5 CONCLUSIONS

This paper presented a novel eccentricity compensation strategy using feed drive modulations. It is shown that by adding a circular trajectory motion at spindle frequency to the tool's original trajectory, the trajectory of geometrical and rotational tool center will match resulting in eliminating the tool eccentricity. An adaptive strategy is proposed to automatically compensate for the eccentricity considering the feed drive dynamics. As a result, the chip load and overall cutting force are evenly distributed across all the flutes of the cutter.

6 REFERENCES

[Ariyur 2003] Ariyur, K. B. and Krstic, M. Real-time optimization by extremum-seeking control. John Wiley & Sons, 2003.

[Buj-Corral 2011] Buj-Corral, I., et al. Influence of feed, eccentricity and helix angle on topography obtained in side milling processes. International Journal of Machine Tools and Manufacture, 2011, vol. 51, no. 12, pp. 889-897. ISSN 0890-6955.

[Farhadmanesh 2021] Farhadmanesh, M. and Ahmadi, K. Online identification of mechanistic milling force models. Mechanical Systems and Signal Processing, 2021, vol. 149, pp. 107318, ISSN 0888-3270.

[Liang 1994] Liang, S. Y. and Perry, S. A. In-Process Compensation for Milling Cutter Runout via Chip Load Manipulation. Journal of Engineering for Industry, 1994, vol. 116, no. 2, pp. 153-160. ISSN 0022-0817.

[Sastry 2000] Sastry, S., et al. Compensation of progressive radial run-out in face-milling by spindle speed variation. International Journal of Machine Tools and Manufacture, 2000, vol. 40, no.8, pp. 1121-1139. ISSN 0890-6955.

[Schmitz 2004] Schmitz, T. L., et al. The Role of Cutter Eccentricity on Surface Finish and Milling Forces. In: ASME International Mechanical Engineering Congress and Exposition, Anaheim, California, USA, November 2004. ASME, pp. 1011-1018.

[Schmitz 2007] Schmitz, T. L., et al. Runout effects in milling: Surface finish, surface location error, and stability. International Journal of Machine Tools and Manufacture, 2007, vol. 47, no. 5, pp. 841-851. ISSN 0890-6955.

[Stevens 1995] Stevens, A. J. and Liang, S. Y. Runout rejection in end milling through two-dimensional repetitive force control. Mechatronics, 1995, vol. 5, no.1, pp. 1-13. ISSN 0957-4158.

[Takahei 2022] Takahei K., et al. Identification of the model parameter for milling process simulation with sensor-integrated disturbance observer. Precision Engineering, 2022, vol 78, pp. 146-162. ISSN 0141-6359.